THE AMERICAN SOCIETY OF MECHANICAL ENGINEERS
345 E. 47th St., New York, N.Y. 10017

93-GT-25

EFFECTS OF FREE-STREAM TURBULENCE INTENSITY ON A BOUNDARY LAYER RECOVERING FROM CONCAVE CURVATURE EFFECTS

Michael D. Kestoras and Terrence W. Simon
Department of Mechanical Engineering
University of Minnesota
Minneapolis, Minnesota

ABSTRACT

Experiments are conducted on a flat recovery wall downstream of sustained concave curvature in the presence of high free-stream turbulence (TI~8%). This flow simulates some of the features of the flow on the latter parts of the pressure surface of a gas turbine airfoil. The combined effects of concave curvature and TI, both present in the flow over a turbine airfoil, have so far little been studied. Computation of such flows with standard turbulence closure models has not been particularly successful. This experiment attempts to characterize the turbulence characteristics of this flow. In the present study, a turbulent boundary layer grows from the leading edge of a concave wall then passes onto a downstream flat wall. Results show that turbulence intensities increase profoundly in the outer region of the boundary layer over the recovery wall. Near-wall turbulent eddies appear to lift off the recovery wall and a "stabilized" region forms near the wall. In contrast to a low-free-stream turbulence intensity flow, turbulent eddies penetrate the outer parts of the "stabilized" region where sharp velocity and temperature gradients exist. These eddies can more readily transfer momentum and heat. As a result, skin friction coefficients and Stanton numbers on the recovery wall are 20% and 10%, respectively, above their values in the low-free-stream turbulence intensity case. Stanton numbers do not undershoot flat-wall expectations at the same $Re_{\Delta 2}$ values as seen in the low-TI case. Remarkably, the velocity distribution in the core of the flow over the recovery wall exhibits a negative gradient normal to the wall under high free-stream turbulence intensity conditions. This velocity distribution appears to be the result of two effects: 1) cross transport of kinetic energy by boundary work in the upstream curved flow and 2) readjustment of static pressure profiles in response to the removal of concave curvature.

NOMENCLATURE

C_f	Skin friction coefficient.
C_{f0}	Skin friction coefficient at very low turbulence intensity.
Cp	Constant-pressure specific heat ratio.
Cp_c	Static pressure coefficient, $(P-Pref)/(0.5\rho U_{cw}^2)$.
H	Shape factor δ_1/δ_2.
L_∞^u	Free-stream length scale $L_\infty^u = \left(\overline{u_\infty^2}\right)^{\frac{3}{2}} \Big/ \left(U_\infty \dfrac{\overline{du_\infty^2}}{dx}\right)$
P	Static pressure
P_d	Dynamic pressure, $P_d = 1/2\rho U^2$
Pr	Molecular Prandtl number.
Pref	Static pressure at the most upstream pressure tap 2 cm from the concave surface
P_t	Total pressure, $P_t = P + P_d$
q_w	Convective heat flux at the wall.
R	Radius of curvature (negative for a concave surface).
Re_x	Reynolds number based upon distance from the beginning of the test wall.
$Re_{\delta 1}$	Reynolds number based upon displacement thickness.
$Re_{\delta 2}$	Reynolds number based on momentum thickness.
St	Stanton number, $St = q_w/\rho C_p (T_w - T_\infty) U_{cw}$
T	Local mean temperature.
TI	Free-stream turbulence intensity $\left(\sqrt{\overline{u^2}}/U_{cw}\right)$
T_∞	Free-stream temperature.
T_w	Wall temperature.
T^+	Temperature in wall units $((T_w-T)/(Tw-T_\infty))\sqrt{Cf/2}/St$.
U	Mean streamwise velocity.
U_c	Local mean velocity obtained by extrapolating the velocity distribution in the core of the flow.
$\sqrt{\overline{u^2}}$	Root-mean-square fluctuation of streamwise velocity.
$\sqrt{\overline{u_\infty^2}}$	Root-mean-square fluctuation of free-stream velocity.
U_p	Potential flow velocity.
U_∞	Free-stream mean velocity
U_{cw}	Value of U_c at the wall.
U^+	Velocity in wall coordinates $U^+ = U/U_\tau$.
U_τ	Shear velocity.
x	Streamwise distance from the leading edge of the concave wall.
y	Distance normal to the wall.
y^+	Normal distance from the wall in wall units, $y^+ = yU_\tau/\nu$.

Presented at the International Gas Turbine and Aeroengine Congress and Exposition
Cincinnati, Ohio May 24–27, 1993
This paper has been accepted for publication in the Transactions of the ASME
Discussion of it will be accepted at ASME Headquarters until September 30,1993

Greek Symbols

β Multiplier accounting for the Reynolds number effect on skin friction coefficients in the presence of high TI effects, $\beta = 3\exp(-Re_{\delta_2}/400) + 1$.

δ Momentum boundary layer thickness.

δ_0 Boundary layer thickness at the entrance to the recovery or concave wall.

δ_1 Displacement thickness.

δ_2 Momentum thickness.

$\delta_{99.5}$ Boundary layer thickness based on 99.5% of the local U_c.

Δ_2 Enthalpy thickness.

Δ_3 Clauser thickness $\Delta_3 = \int_0^\infty \left((U_p - U)/U_\tau\right) dy$.

$\Delta_{99.5}$ Thermal boundary layer thickness based on 99.5% of the wall-to-free-stream temperature difference.

ΔC_f Change in skin friction coefficient relative to the zero TI value, $\Delta C_f = C_f - C_{f0}$.

θ Angular position around the bend.

ν Molecular kinematic viscosity.

ρ Density.

INTRODUCTION

The effects of high free-stream turbulence intensity have been under study for more than 30 years. Early studies (e. g. Kestin, 1966 and Feiler and Yeager, 1962 reported conflicting results on the effects of high TI on heat transfer over a flat plate for TI in the range (0.7%-8%). Simonich and Bradshaw (1978) suggested that the conflicting results are due mainly to a Reynolds number effect, the effect diminishing as the Reynolds number increases. They noted a 5% increase in Stanton number for every 1% increase in free-stream turbulence intensity (TI < 7%) at Re_{δ_2}=6500 (relatively high). Elevated TI suppressed the wake of temperature profiles, the effect increasing with increased TI. The results section of this paper will show that the wake of temperature profiles over the recovery wall is also suppressed by high TI. Hancock and Bradshaw (1983) observed that the free-stream length scale, L^u_∞ is also important in describing the effects of free-stream turbulence. They found that the empirical parameter, $\left(\sqrt{u^2}/U\right)_\infty \times 100 \Big/ \left(L^u_\infty/\delta_{99.5} + 2.0\right)$ correlates changes in skin friction coefficients, $(C_f - C_{f0})/C_{f0}$ quite satisfactorily. Blair (1983) conducted experiments in a heated turbulent boundary layer over a flat plate. He stated that the effects of elevated TI follow the functional relation $\Delta(C_f, St, U(y), T(y)) = f\left(\sqrt{u^2_\infty}/U_\infty, L^u_\infty/\delta_{99.5}, Re_{\delta_2}\right)$ and extended Hancock's correlation by including an empirical term, $\beta = 3\exp(-Re_{\delta_2}/400) + 1$ as a multiplier to Hancock's correlating term to account for low Re_{δ_2} effects. He also observed that the logarithmic regions in velocity and temperature profiles were unaffected by free-stream turbulence intensity. As shown in the present work, the logarithmic region of a boundary layer over a recovery wall also remains unaffected by the elevated TI.

Data on the effects of TI on turbulent boundary layers over curved surfaces are very limited. Brown and Burton (1977) reported no effect of TI (1.6%-9.2%) on Stanton numbers over convexly-curved surfaces. You et al. (1986) studied the effects of two levels of free-stream turbulence intensity (0.65%-1.85%) on a heated turbulent boundary layer over a convex surface for which $\delta_{99.5}/R$=0.03. They reported that free-stream turbulence intensity enhances the stabilizing effects of convex curvature on mean and turbulence quantities.

Data on the effects of TI on turbulent boundary layers over a concave wall are few. Nakano et al. (1981) studied the effects of stable free-stream flow (positive shear) and unstable free-stream flow (negative shear) on a turbulent boundary layer over a concave wall. Under unstable free-stream flow conditions, shear-stress values in the boundary layer over the concave wall increase relative to values under stable free-stream flow conditions. Kim et al. (1991) reported mean and turbulence measurements over the same concave wall used in the present study. In the high-TI case (8%), they reported cross-transport of momentum taking place even in the core of the flow. Kestoras and Simon (1992) reported mean momentum and heat transfer measurements in a boundary layer recovering from sustained concave curvature under low-TI conditions (TI=0.6%). Skin friction coefficients dropped abruptly at first, slowly thereafter, approaching flat-wall values. Stanton numbers showed a similar behavior, with one important difference: they quickly dropped below flat-wall values, then reached near-constant values and remained well below equivalent flat-wall values by the end of the test section, $33\delta_0$ from the bend exit. This behavior was attributed to a thickening of the viscous sublayer and a lifting of the large-scale eddies off the wall. Velocity and temperature profiles reached a self-preserving shape over the recovery wall, exhibiting unusually sharp gradients near the wall.

In the present study, data taken on a flat wall downstream of a concave wall under high-TI conditions are presented. To the authors' knowledge, this is the first time that the combined effects of high free-stream turbulence intensity and recovery from concave curvature are documented.

TEST FACILITY AND INSTRUMENTATION

The facility is an open-circuit, blown-type wind tunnel (Fig. 1). Details of the flow delivery section are given by Wang (1984). Measurements are taken at a nominal velocity of 17.2 m/s. This velocity is uniform to within 0.3% across the face of the nozzle. The free-stream temperature of the flow is uniform to within 0.1°C.

A free-stream turbulence intensity of ~8% at the inlet of the test channel is achieved using an insert section downstream of the contraction nozzle (Russ, 1989). This insert consists of a bi-plane grid of 4.2 cm OD PVC pipes on 10.8 cm centers. Downstream of the grid there is a 96.5 cm long development region. The grid is similar to that used by O'Brien and vanFossen (1985). Data show that turbulence decays more quickly with streamwise distance on the upstream part of the concave wall. On the recovery wall, the decay of turbulence is very slow (TI ~ 4%). A power

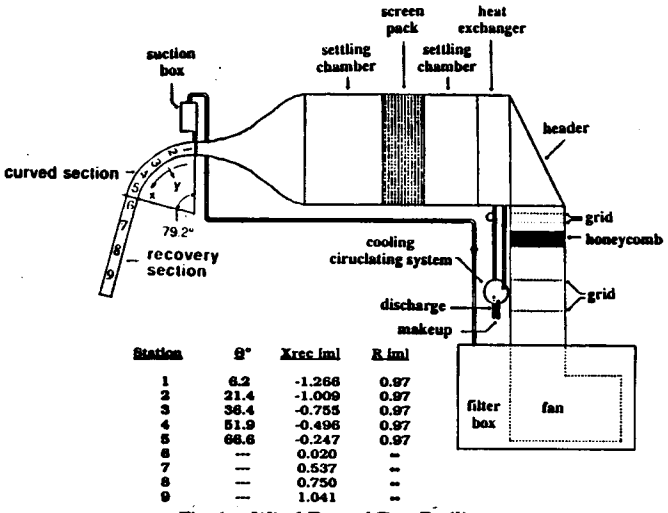

Station	θ°	Xrec [m]	R [m]
1	6.2	-1.266	0.97
2	21.4	-1.009	0.97
3	36.4	-0.755	0.97
4	51.9	-0.496	0.97
5	66.6	-0.247	0.97
6	---	0.020	∞
7	---	0.537	∞
8	---	0.750	∞
9	---	1.041	∞

Fig. 1 Wind Tunnel Test Facility

density spectrum taken at the nozzle exit shows that 19.6% of the turbulent energy in the free-stream is distributed over frequencies which are below 25 Hz.

The test channel is rectangular, 68 cm wide, 11 cm deep, and 284 cm long. The test wall consists of two major segments (concave wall and recovery wall) which are designed and assembled to provide a smooth, uniformly-heated surface. Both segments were fabricated similarly. For example, the recovery wall consists of a layer of fiberglass insulation, a sheet of Plexiglas, an electrical resistance heater, a thin spacer, a stainless steel sheet, and, adjacent to the flow, a layer of liquid crystal. Thermocouples embedded into the spacer are distributed both in the streamwise and spanwise directions.

The concave wall has a radius of 0.97 m and is 1.38 m long. The recovery wall is 1.452 m long and is tangent to the concave wall. The outer wall is adjusted to obtain negligible streamwise acceleration: static pressure coefficients, Cp_c, are kept to within 0.03 for the entire test length. Such Cp_c values are based upon static pressures taken at a radial distance of 2 cm from the test wall. Static pressures were measured using an array of static pressure taps on an end wall. The taps were distributed both in the x and y directions.

At the entry to the recovery section Re_x, $Re_{\delta 1}$ and $Re_{\delta 2}$ are 1.4 X 10^6, 1487 and 1174, respectively.

Data acquisition and processing are performed by a Hewlett Packard series 200, Model 16 personal computer. Mean and fluctuating velocities are measured using a hot -wire (TSI 1218-T1.5) probe on which the prongs are bent 90° to the probe holder to minimize flow interference. A constant-temperature, four-channel bridge (TSI-IFA-100) is used to power the hot-wires. Analog output signals are digitized using an HP3437A system voltmeter. For statistical quantities, the sampling rate is 100 Hz and the sampling duration is at least 40 seconds.

Velocities are measured when the walls are not heated. The free-stream temperature is continuously monitored and the hot-wire voltage output is corrected for any temperature variations. The uncertainty in $\overline{u^2}$ is 3%.

Heat transfer experiments are conducted with the test walls uniformly heated to nominally 193 W/m^2 within a 1% nonuniformity (Wang, 1984). Wall temperatures are measured with 76 μm diameter embedded chromel-alumel thermocouples. The thermocouples were calibrated against a platinum-resistance standard. The spacings of the thermocouples in the streamwise direction are 2.54 and 5.08 cm over the concave and recovery walls, respectively. Surface temperatures are obtained by correcting the thermocouple readings for temperature drops between the embedded thermocouple beads and the test wall surface. Such corrections for the concave and the recovery walls, respectively, were typically 1.2°C and 0.3 of the 5.5°C thermocouple-to-free-stream temperature difference. The uncertainty in the wall temperature readings, thus obtained, is 0.2°C. Careful measurements of wall material conductivity, contact resistance values, and surface emissivity were needed to achieve this uncertainty. An energy balance was performed by comparing the enthalpy thicknesses calculated from the measured velocity and temperature profiles and the enthalpy thicknesses obtained by integration in the streamwise direction of wall values. On the concave wall, where the wall temperature correction is largest, a closure within 5% was obtained.

Profiles were taken using a stepping motor assembly. The motor is capable of 400 half-steps per revolution, each half-step equivalent to 5 μm of travel in the y- direction.

Determination of $\delta_{99.5}$ presents some difficulty in the high-turbulence case: no analytical equation is available for determining the velocity distribution outside the boundary layer over the recovery wall. The velocity distribution in the core of the flow is different from the distribution in a low-turbulence case, primarily because of cross transport of momentum by boundary work over the upstream concave wall (Eckert, 1987). Eckert suggests that this cross transport of momentum is dependent on the unsteadiness of the flow and the bending of the flow path-lines. Both factors are nearly constant across the core of the flow over the upstream concave wall: This implies a nearly uniform cross transport of momentum across the channel toward the concave wall but outside the boundary layer. Though the slope of the linear distribution of velocities in the core of the flow over the concave wall changes from that observed in a low-turbulence case (Kestoras and Simon, 1992) the velocity distribution in the core of the flow remains linear when high TI is introduced. The velocity profile in the core of the flow throughout the recovery section also remains linear. In this work, velocities in the core of the flow are least-square fitted with a straight line, capitalizing on this linearity; the resulting equation is used to provide the velocities that would be obtained in the vicinity of the wall if the boundary layer were not present. The velocities, thus obtained, are used instead of U_p (used previously in the low-turbulence cases) to determine $\delta_{99.5}$, δ_1, and δ_2).

RESULTS

Under high free-stream turbulence conditions (TI≈8%) the flow appears fully turbulent, in terms of the wall skin friction and heat transfer, from the leading edge of the concave wall. Stable Görtler-like vortices do not appear in the high-turbulence case, in contrast to a previous case taken under low-TI conditions. Spanwise non-uniformities, which would indicate the presence of such vortices, do not appear on the liquid crystal covering the test surface; moreover, spanwise profiles of streamwise mean velocity do not show the maxima or minima observed in the low-turbulence case. Turbulence measurements (Kestoras, 1993) indicate that a scenario whereby Görtler-like vortices exist but meander with time may not be correct. Indeed, it appears that there is no coherent vortex activity. The effects of high TI are most profound in the outer region of the boundary layer over the recovery wall. In the inner region, the high-TI effects are important but the removal of concave curvature is more influential.

The structural changes of the boundary layer over the upstream concave wall, brought about by high TI, can be described as follows: at the bend exit, the near-wall velocity profiles exhibit sharper gradients than in a low-TI case. These sharp velocity gradients are the result of the following two effects taking place over the concave wall: 1) High free-stream turbulence provides large-scale, high-streamwise-momentum eddies outside the boundary layer. These eddies are accelerated towards the concave surface and induce an increase in eddy scale within the boundary layer. 2) Cross transport of energy by boundary work proceeds even outside of the boundary layer over the concave wall (Eckert, 1987) raising the streamwise momentum near the wall.

This paper documents the effects of the removal of concave curvature under high-TI conditions. Measurements are presented and their significance discussed. Effects of TI are isolated by comparing with data from a low-TI case (Kestoras and Simon, 1992, TI=0.6%). Important parameters of the study are shown in Table 1.

Non-Dimensional Velocity Profiles

Non-dimensional velocity profiles over the recovery wall (stations 7H-9H) are shown in Figure 2. The velocity profile taken over the concave wall, 24 cm upstream of the bend exit (station 5H), is also shown for comparison. On the recovery wall, the velocity profiles in the core of the flow exhibit negative gradients whereas the profile gradient at station 5H is positive outside the boundary layer (Fig. 2). This unexpected behavior may be explained as follows: On the concave wall, cross transport of energy takes place in the core of the flow toward the concave wall resulting in total pressure profiles that increase towards the concave surface (Kestoras, 1993). This cross transport in the core of the flow requires streamline curvature as discussed by Eckert (1987). It is, thus, shut off on the recovery section. The total pressure distribution profile at the bend exit is essentially maintained throughout the recovery section since no efficient means for transport remains. Readjustment to flat-wall static pressure profiles (centrifugal forces are removed) results in dynamic pressure ($P_d=P_t-P$) profiles with negative y-gradients. Thus, the

	Station 4H	Station 5H	Station 6H	Station 7H	Station 8H	Station 9H
x (m)	0.875	1.133	1.390	1.912	2.124	2.416
R (cm)	97	97	∞	∞	∞	∞
U_{cw} (m/s)	16.71	17.09	16.41	17.17	16.77	16.95
$T.I._{core}$	5.201	4.631	4.618	4.150	4.135	4.127
$\delta_{99.5}x10^2$(m)	3.87	3.60	2.40	2.69	2.86	2.89
$\delta_1 x10^3$(m)	1.987	2.129	1.452	2.052	2.308	2.473
$\delta_2 x10^3$(m)	1.618	1.746	1.146	1.586	1.776	1.411
$(y/\delta_{99.5})_{y+=10}$	0.006	0.005	0.008	0.007	0.007	0.007
$R_{ex}x10^5$	9.44	12.05	14.23	20.84	23.26	25.68
$Re_{\delta 1}$	2144	2264	1487	2236	2527	2630
$Re_{\delta 2}$	1746	1857	1174	1728	1944	2033
H	1.228	1.219	1.267	1.294	1.300	1.294
$C_f x10^3$	5.00	4.93	4.85	4.45	4.36	4.19
$(\partial U/\partial y)_{core}$	10.1	15.4	15.7	-10.1	-9.5	-9.6
$\Delta_{99.5}$(cm)	3.312	4.538	6.062	6.157	7.693	8.817
Δ_2(mm)	1.602	2.372	2.478	2.304	4.042	4.104
T_∞	27.74	27.77	27.74	27.68	27.60	27.67
T_w(c)	31.32	31.35	31.74	31.94	31.88	32.13
$Re_{\Delta 2}$	1662	2517	2521	2451	4203	4310
q_w	165.6	165.4	172.1	163.8	163.6	162.6
St $x10^3$	2.376	2.321	2.251	1.922	1.957	1.846
$2St/C_f$	0.951	0.941	0.928	0.864	0.898	0.881

Table 1. Boundary Layer Parameters. Concave-Wall Stations 4H and 5H; Joint: Station 6H; Recovery wall Stations 7H-9H.

velocity profile ($P_d = 0.5\rho U^2$) also exhibits a negative y-gradient.

After the removal of curvature, the boundary layer thicknesses, $\delta_{99.5}$, δ_1 and δ_2 decrease (Station 7H in Table 1). Values of $\delta_{99.5}$, δ_1 and δ_2 increase monotonically for the rest of the recovery wall. Their values however, do not rise above the pre bend-exit value (station 5H) before the mid-downstream location of the recovery wall (station 8H). It therefore appears that there is a mechanism in the vicinity of the bend exit which transports streamwise momentum away from the wall quite efficiently. Before the bend exit (station 5H in Fig. 2) streamwise momentum increases with y. By conservation of angular momentum, the fluid layers with the higher streamwise momentum may tend to lift off the test wall whereas fluid layers close to the surface show a smaller tendency to lift off. This impulse of cross transport of momentum away from the test wall in the vicinity of the bend exit is consistent with the readjustment of the shape of the local velocity profiles. At the joint between the concave and recovery walls (station 6H), the near-wall, $y/\delta_{99.5} < 0.03$ velocity gradient, is shallower than for the upstream profiles (stations 4H and 5H in Fig. 3). This may at first seem strange since readjustment of static pressure profiles would tend to produce near-wall acceleration at this point. It is believed to be a result of the lifting of the vortices.

As with the low-TI case, the recovery wall velocity profiles assume a near-asymptotic shape (stations 7H-9H in Fig. 4). This behavior is especially true near the wall $y/\delta_{99.5} < 0.13$. Moreover, near the wall ($y/\delta_{99.5} < 0.13$), self-similarity is established by station 6H (only 2 cm downstream of the bend exit, not shown in the Fig. 4) suggesting that the redistribution of momentum discussed above begins slightly upstream of the bend exit and is complete soon after the beginning of recovery.

High-TI results in velocity profiles (e.g. station 8H in Fig. 5) which are fuller than profiles under low-TI conditions (stations 8U and 8D). It is remarkable, however, that the near-wall velocity profiles, $y/\delta_{99.5} < 0.01$, (insert in Fig. 5) are the same for all. This near-wall similarity, because of its importance in determining mean and turbulence quantities, appears to be the reason for the many common features over the recovery wall for both the high- and low-TI cases. It will be shown later that a "stabilized" region appears near the recovery-wall. It is presumed that, for the most part, the "stabilized" region is depleted of turbulent eddies and, therefore, should be little affected by the external high TI. It can therefore be argued that, since the velocity profile in the region ($y/\delta_{99.5} < 0.01$) remains unaffected by elevated TI, the "stabilized" region is about one-hundredth of the boundary layer thickness.

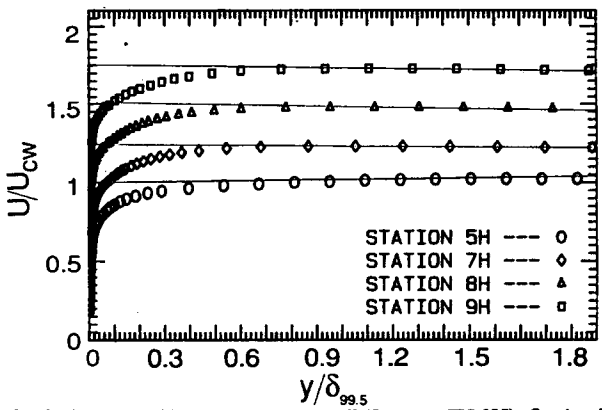

Fig. 2 Velocity Profiles on Recovery Wall (Stations 7H-9H). Station 5H; Concave Wall. Profiles Shifted in the Vertical Direction

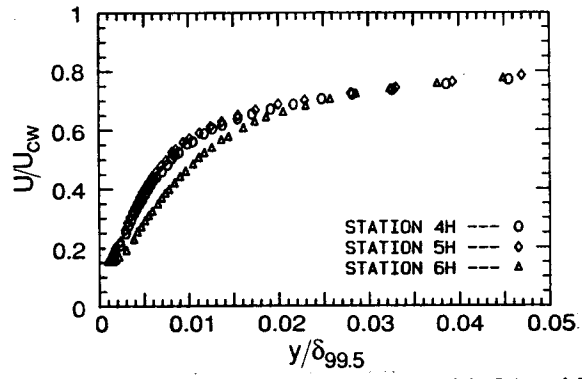

Fig. 3 Near-Wall Velocity Profiles in the Vicinity of the Joint of the Concave and Recovery Walls.

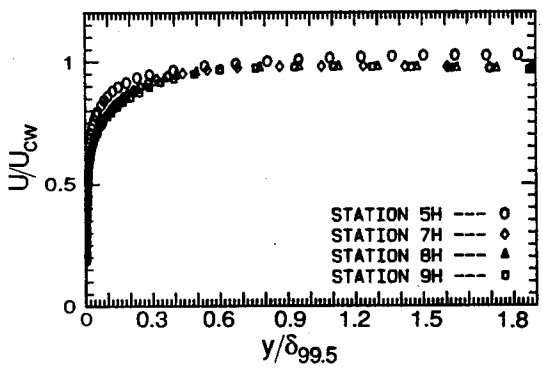

Fig. 4 Asymptotic Behavior of Velocity Profiles on the Recovery Wall under High-TI Conditions (Stations 7H-9H).

Velocity Profiles in Wall Coordinates

Over the recovery wall, the law of the wall appears to be valid up to y^+~300 (stations 7H-9H, Fig. 6) whereas over the concave wall, the logarithmic region extends only to y^+~80 (Kestoras, 1993). Similar enlargement of the logarithmic region over the recovery wall was observed in the low-TI case (e.g. stations 8U and 8D in Fig. 7). Elevated TI appears to affect only the wake region of the velocity profile in wall coordinates. Negligible effects of TI on the logarithmic region of a velocity profile were also reported in boundary layers over a flat plate (Blair, 1983).

The wake, suppressed in the high-TI case over the concave wall (Kestoras, 1993), begins to reestablish very early after the removal of curvature (station 6H, not shown) and continues to do so throughout the recovery wall (stations 7H-9H, Fig. 6). Nevertheless, a negative wake

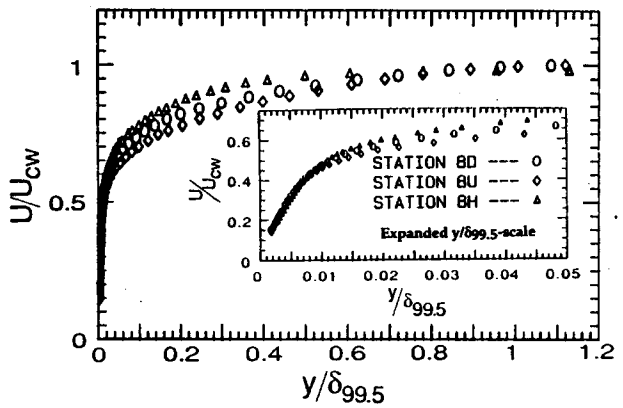

Fig. 5 Effect of High TI on Non-Dimensionalized Velocity Profiles at Station 8 on the Recovery Wall. Stations 8U and 8D; Upwash and Downwash Sites of Görtler-Like Vortices--Low-TI case. Station 8H; High-TI Case.

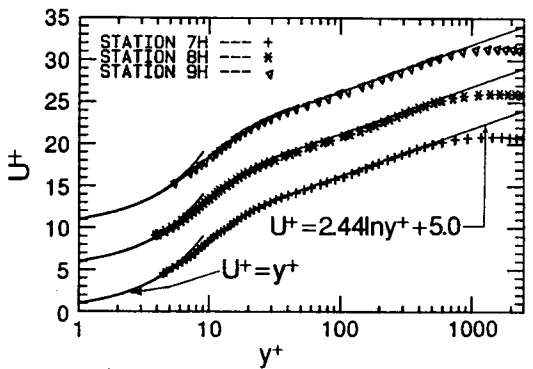

Fig. 6 Streamwise Evolution of Mean Velocity Profiles on the Recovery Wall in Wall Coordinates.

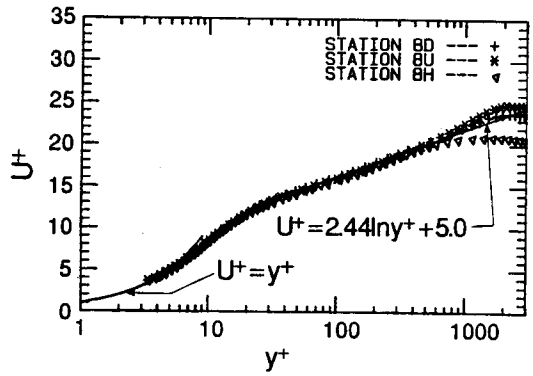

Fig. 7 Effect of High TI on Velocity Profiles on the Recovery Wall in Wall Coordinates. Stations 8U and 8D; Upwash and Downwash Sites of Görtler-Like Vortices--Low-TI case. Station 8H; High-TI Case.

persists (see station 9H). Similar reemergence of the wake is observed in the low-TI case (Kestoras and Simon, 1992). However, the persistence of negative wakes over the recovery wall in the high-turbulence case (station 8H in Fig. 7 , for example) is in contrast to the positive wakes exhibited under low-TI conditions (station 8U and 8D).

Velocity Profiles in Outer-Region Similarity Coordinates

The experiment is conducted under a condition of negligible streamwise acceleration and thus, would display equilibrium boundary layer characteristics under flat-wall conditions. Equilibrium boundary layers exhibit outer-region similarity when plotted in the coordinates of Fig. 8 . Thus, if the residual effects of curvature would not preclude such behavior, the self similarity exhibited over the recovery wall (stations 7H, 8H, and 9H) in the outer region ($y/\Delta_3>0.1$) is expected. However, self similarity is also exhibited in the inner region. Velocity profiles in the low-TI case also exhibit both inner- and outer-region similarity. As explained by Kestoras and Simon (1992), this inner-region similarity may be an implication of the existence of a "stabilized" region near the recovery wall. Similar behavior was observed in strongly-accelerated boundary layers where a near-wall "stabilized" layer ("laminar-like") was also documented (Kays and Moffat, 1975).

Streamwise Turbulence Intensity Profiles

At the bend exit, turbulence intensity values in the presence of high TI (station 7H-9H in Fig. 9) drop only slightly from the enhanced concave-wall values (station 5H). This reduction is only one-tenth the reduction observed between the same stations in the low-TI case

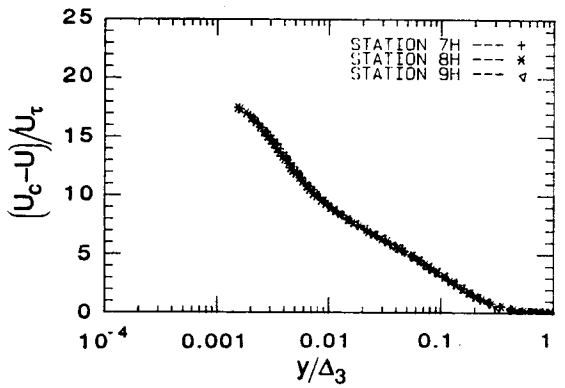

Fig. 8 Inner- and Outer-Region Similarity Exhibited by Velocity Profiles on the Recovery Wall under High-TI Conditions.

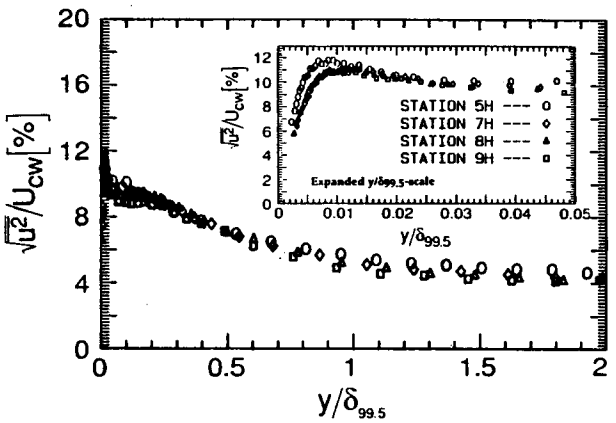

Fig. 9 Streamwise Evolution of Turbulence Intensities on the Concave Wall (Station 5H) and Recovery Wall (Stations 7H-9H).

(Kestoras and Simon, 1992). It appears that the turbulent eddies at the edge of the boundary layer are large enough to dominate both the core of the flow and the boundary layer flow.

Near the surface of the recovery wall, $y/\delta_{99.5}<0.012$ (insert in Fig. 9), turbulence intensity profiles do assume a self-similar shape (stations 7H-9H). This self-similar shape first appears at station 6, only 2 cm downstream of the bend exit (not shown). Turbulence intensity values under high-TI conditions deviate from those in the low-TI case for $y/\delta_{99.5} > 0.006$ (Fig. 10, only station 8 is shown). This may indicate that turbulent eddies penetrate deeper into the "stabilized" region under high-TI conditions. Deeper penetration couples the turbulent eddies with the sharp velocity gradients in this region, resulting in more efficient transport of momentum and, thus, a quicker recovery.

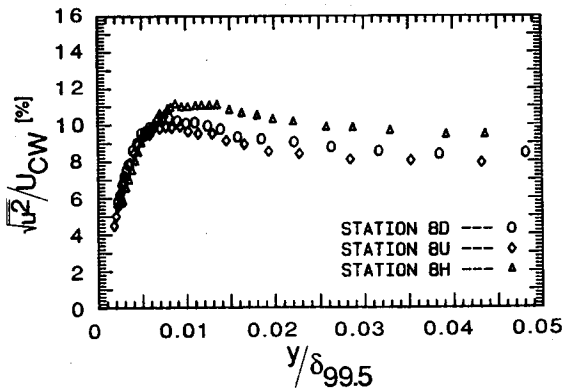

Fig. 10 Effect of High TI on Near-Wall Turbulence Intensities on the Recovery Wall. Stations 8U and 8D; Upwash and Downwash Sites of Görtler-Like Vortices–Low-TI case. Station 8H; High-TI Case.

Immediately after the bend exit, the viscous sublayer appears to grow faster than does $\delta_{99.5}$, indicated by near-wall turbulence intensity profiles in insert in Fig. 9 where lower near-wall gradients are shown for stations 7H-9H than for 5H. This may indicate a thickening of the viscous sublayer after the bend exit which is consistent with observations in temperature profiles (to be presented). A thickening of the viscous sublayer upon recovery is also observed in the low-TI case. The peaks in profiles 7H-9H are at the same location for both low- and high-TI cases, indicating that the eddies lift off the recovery wall in a manner that is independent of TI.

Non-Dimensionalized Mean Temperature Profiles:

On the recovery wall, temperature profiles (stations 7H-9H, Fig. 11) exhibit a near-self-similar behavior starting from the exit of the bend. Similar behavior was also observed in the low-TI case (Kestoras and Simon, 1992).

High free-stream turbulence effects fuller mean temperature profiles on the recovery wall (Fig. 12) than in the low-TI case. The innermost 20% of the boundary layer accounts for almost 95% of the wall-to-free-stream temperature difference; less than 85% in the low-TI case. Such a high near-wall thermal resistance indicates a "stabilized" layer, as reported in the low-TI case (Kestoras and Simon, 1992). However, in the presence of high TI, temperatures in the region are higher than values under low-TI conditions (insert in Fig. 12). Furthermore, temperature profiles in the inner part of the "stabilized" region ($y/\delta_{99.5} < 0.005$) possess sharper gradients (station 8H in insert in Fig. 12) than temperature profiles in the low-TI case (stations 8U and 8D). In contrast, velocity profiles in the near-wall region ($y/\delta_{99.5} < 0.01$ in insert in Fig. 5) are not affected by TI level.

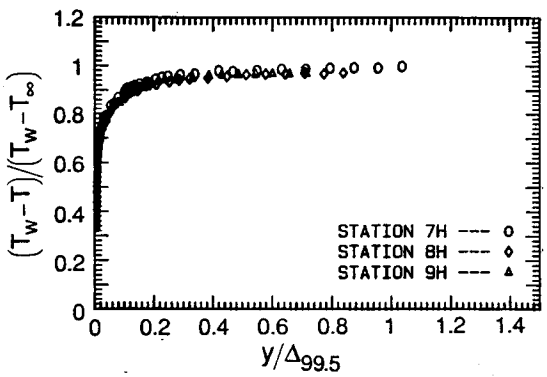

Fig. 11 Asymptotic Behavior of Non-Dimensionalized Mean Temperature Profiles on the Recovery Wall under High-TI Conditions.

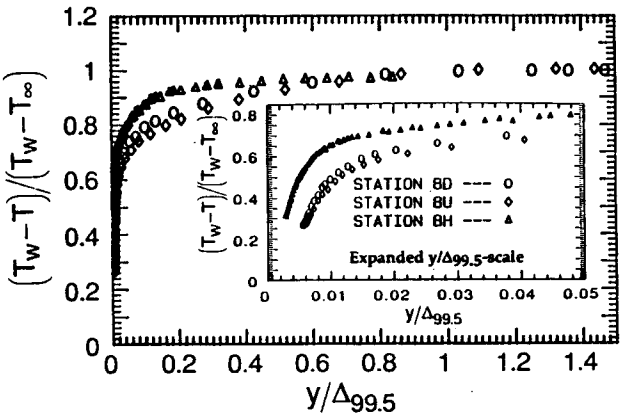

Fig. 12 Effect of High TI on Non-Dimensionalized Mean Temperature Profiles on the Recovery Wall under High-TI Conditions. Stations 8U and 8D; Upwash and Downwash Sites of Görtler-Like Vortices--Low-TI case. Station 8H; High-TI Case.

Temperature Profiles in Wall Coordinates

Temperature profiles (stations 7H-9H in Fig. 13) show little evolution in the conduction layer and the logarithmic region under high-TI conditions. However, the wake appears to be slowly reemerging. Over the concave wall, the wake is suppressed by high TI and concave curvature (Kestoras, 1993). A reemergence of the wake on the recovery wall is also observed in the low-TI case (Kestoras and Simon, 1992).

A thickening of the conduction layer appears at the joint between the concave and recovery walls. To indicate this increase, the y^+-position where the conduction layer equation, $T^+=Pr\ y^+$, first departs from the data is marked, for each station (Fig. 13) and vertical lines C and D are drawn to indicate these points for station 5H, and for stations 6H, 7H, 8H and 9H, respectively. A single line suffices for the last four stations. The locations of lines C and D can be taken as measures of the thicknesses of the respective conduction layers. The conduction layer thicknesses rise at the end of the bend, then remain the same throughout the recovery wall length. A thickening of the conduction layer after the bend exit is also observed in the low-TI case. It appears that free-stream turbulence has a minimal effect in the inner part of the boundary layer.

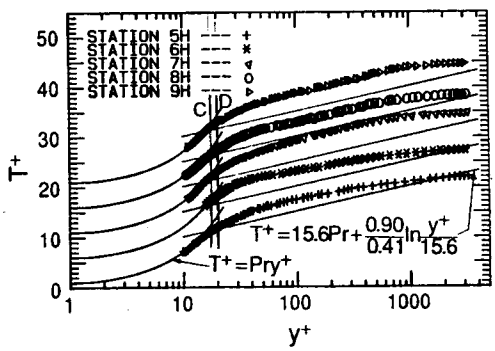

Fig. 13 Streamwise Evolution of Mean Temperature Profiles in Wall Coordinates on the Recovery Wall (Stations 7H-9H). Concave Wall; Station 5H; Joint Station 6H.

Friction Coefficients

On the recovery wall, the effect of elevated TI on skin friction coefficients is very profound (Fig. 14). In the low-TI case, skin friction coefficients at the bend exit drop as much as 20% from the enhanced concave-wall values. In contrast, the corresponding drop in the high-TI case is only 8%. Thus, skin friction coefficients on the recovery wall increase by 20% when TI is elevated. This sensitivity to TI may be caused by penetration of eddies into the outer part of the "stabilized" region. Effective mixing, resulting from the coupling of the penetrating eddies

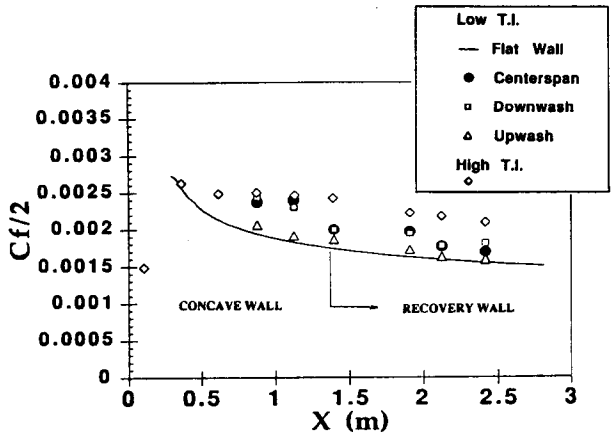

Fig. 14 Skin Friction Coefficients on the Concave and the Recovery Walls. Centerspan, Downwash and Upwash are the Respective Sites of Görtler-Like Vortices; Low-TI Case. Flat-Wall Line calculated using Mixing Length Modeling.

with the sharp velocity gradients in the "stabilized" region greatly boosts the cross-stream transport of momentum.

Stanton Numbers

Stanton numbers show that the boundary layer is turbulent-like essentially from the leading edge of the concave wall (Fig. 15). In contrast, a transition zone is present under low-TI conditions (Kestoras and Simon, 1992).

The response of Stanton numbers to elevated TI on both the concave and recovery walls (Fig. 15) is similar to the response of skin friction coefficients. On the recovery wall, Stanton numbers rise 10%

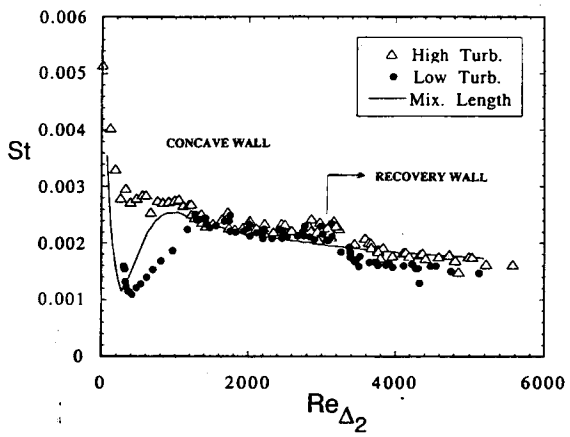

Fig. 15 Comparison of Streamwise Behavior of Stanton Numbers under Low- and High-TI Conditions. Flat Wall Expectations calculated Using Mixing Length Modeling.

when TI is elevated, half the corresponding increase in skin friction coefficients.

As in the low-TI case, Stanton numbers drop at the bend exit, then level off, assuming a near-constant value for the remainder of the recovery wall. The qualitative similarity in Stanton numbers of the two cases may be a result of dominance of near-wall phenomena which appear to be independent of TI. Such a phenomenon is the thickening of the conduction layer, which adversely affects heat transfer (Kays and Moffat, 1975).

The high Stanton numbers on the recovery wall in the high-TI case may be the result of turbulent eddies penetrating the "stabilized" region, where velocity gradients are sharper. Temperature profiles, however, exhibit sharper gradients in the inner part and shallower gradients in the outer part of the "stabilized" region under high-TI conditions Therefore, the eddies that penetrate the outer parts of the "stabilized" region do not enhance heat transfer as much as they enhance momentum transfer. Thus, over the recovery wall, the increase in Stanton numbers with elevated TI is only half the increase in skin friction coefficients.

CONCLUSIONS

In this study the combined effects of high TI and the removal of concave curvature are documented. These data are important for real turbine airfoil flow where high-TI conditions prevail. At the bend exit, the velocity and temperature profiles are fuller than profiles in the low-TI case (Kestoras, 1993). As in the low-TI case, turbulent eddies lift off the recovery wall and the viscous sublayer thickens relative to the boundary layer thickness on the concave wall (Fig. 16). The "stabilized" region remains largely unaffected in the mean by the elevated TI. However, measurements show that turbulent eddies do penetrate the outer layers of the "stabilized" region (Fig. 16). As they do, eddy action on the sharp velocity and temperature gradients of the "stabilized" region result in an increase in momentum and heat transfer. Cross transport of momentum by boundary work, which is active over the concave wall, ceases over the recovery wall. Since turbulent eddies lift off the recovery wall, the momentum which has accumulated near the surface over the concave wall has no efficient way of diffusing away from the wall on the recovery section. As in the low-TI case, this excess momentum persists over the recovery wall (Fig. 16). The main conclusions of this study are:

(1) On the recovery wall, at least part of the "stabilized" region near the surface remains unaffected by elevated TI. Mean velocity profiles in this part of the "stabilized" region show no response to elevated TI.

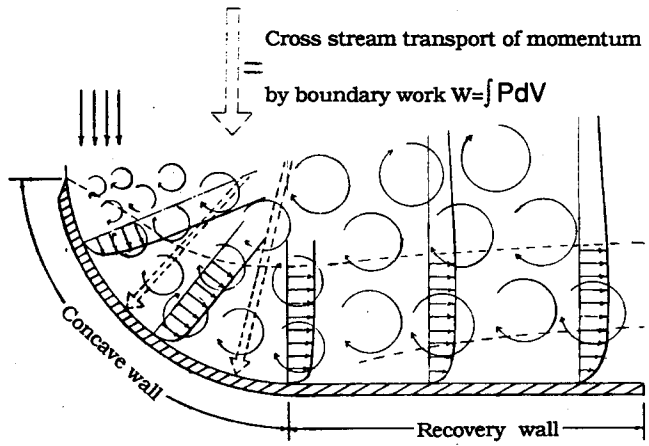

Fig. 16 Schematic Diagram of Structural Changes Effected by Introduction and Removal of Concave Curvature under High-TI Conditions.

(2) Turbulence intensity profiles show that eddies in the high-TI case penetrate the outer 40% of the "stabilized" region. It is suggested that C_f and St values increase substantially over the recovery wall, with enhanced TI because the eddies penetrate this region.

(3) As in the low-TI case, velocity profiles over the recovery wall exhibit inner- and outer-region similarity.

(4) On the recovery wall, sharper temperature gradients are established in the inner layers of the "stabilized" region relative to gradients in the low-TI case. Conversely, gradients in the outer

part of the "stabilized" region are reduced. Thus the effectiveness of the mixing resulting from the eddies penetrating the outer parts of the "stabilized" region is reduced. As a result, heat transfer on the recovery wall does not increase with increased TI as much as does momentum transfer.

(5) The boundary layer over the recovery wall appears to be free of spanwise non-uniformities. It is suggested that Görtler-like vortices do not form under high-TI conditions.

(6) For $y^+ < 300$, the momentum law of the wall remains valid over the recovery wall.

ACKNOWLEDGMENTS

This work was supported by the Air Force Office of Scientific Research. The project (grant number AF/AFOSR-91-0322) monitor is Maj. D. Fant.

REFERENCES

Blair, M. F., (1983), "Influence of Free-Stream Turbulence on Turbulent Boundary Layer Heat Transfer and Mean Profile Development, Part II-Analysis of Results", J. of Heat Transfer, Vol. 105, pp.41-47.

Brown, A., and Burton, R. C., (1977), "The Effects of Free-Stream Turbulence Intensity and Velocity Distribution on Heat Transfer to Curved Surfaces", ASME Paper 77-Gt-48.

Eckert E. R. G., (1987), "Cross Transport of Energy in Fluid Streams," Wärme-und Stoffübertragung, Vol. 21, pp. 73-81.

Feiler, C.E. and Yeager, E.B., (1962), "Effect of Large-Amplitude Oscillations on Heat Transfer", NASA Tech. Report R-142, 1962.

Hancock, P. E., and Bradshaw, P., (1983), "The Effect of Free-Stream Turbulence on Turbulent Boundary Layers", Transactions of the ASME, Vol. 105, pp. 284-289.

Kays, W.M., and Moffat, R.J. (1975) "The Behavior of Transpired Turbulent Boundary Layers", Report HMT-20, Thermosciences Division, Department of Mechanical Engineering, Stanford University.

Kestin, J., (1966), "The Effects of Free-Stream Turbulence on Heat Transfer Rates", Advances in Heat Transfer, Vol. 3, ed. by T.F. Irvine, Jr. and J.P. Hartnett, Academic Press, London 1966.

Kestoras, M.D., and Simon, T.W., (1992), "Hydrodynamic and Thermal Measurements in a Turbulent Boundary Layer Recovering from Concave Curvature," ASME Journal of Turbomachinery, Vol. 114, No. 4, pp. 891-898.

Kestoras, M.D. (1993), "Heat Transfer and Fluid Mechanics Measurements in a Turbulent Boundary Layer Recovering from Concave Curvature", Ph.D. Thesis, University of Minnesota.

Kim, J., Simon, T.W., and Russ, S.G., (1991), "Free-stream Turbulence and Concave Curvature Effects on Heated, Transitional Boundary Layers," ASME J. of Heat Transfer, Vol. 114, No. 2, pp. 339-347.

Nakano, S., Takahashi, A., Shizawa, T. and, Honami, S., (1981), "Effects of Stable and Unstable Free-Streams on a Turbulent Flow Over a Concave Surface", Proc. 3rd Symposium on Turbulent Shear Flows, Davis, CA.

O'Brien, J.E. and vanFossen, G.J. (1985) "The Influence of Jet Grid Turbulence on Heat Transfer from the Stagnation region of a Cylinder in Cross Flow", ASME 85-HT-58.

Russ, S.G. (1989), "The Generation and Measurement of Turbulent Flow Fields", MSME Thesis, Dept of Mech, Engin., University of Minnesota.

Simonich, J. C., and Bradshaw, P., (1978), "Effect of Free-Stream Turbulence on Heat Transfer through a Turbulent Boundary Layer", Transactions of the ASME, Vol. 100, pp. 671-677.

Wang, T., (1984), "An Experimental Investigation of Curvature and Freestream Turbulence Effects on Heat Transfer and Fluid Mechanics in Transition Boundary Layer Flows," PhD Thesis, University of Minnesota.

You, S. M., Simon, T. W., and Kim, J., (1986), "Free-Stream Turbulence Effects on Convex-Curved Turbulent Boundary Layers", Proc. Gas Turbine Heat Transfer Session, ASME Winter Annual Meeting.